

# DeepIPC: Deeply Integrated Perception and Control for Mobile Robot in Real Environments

Oskar Natan<sup>1</sup> and Jun Miura<sup>2</sup>

**Abstract**—We propose DeepIPC, an end-to-end multi-task model that handles both perception and control tasks in driving a mobile robot autonomously. The model consists of two main parts, perception and controller modules. The perception module takes RGB image and depth map to perform semantic segmentation and bird’s eye view (BEV) semantic mapping along with providing their encoded features. Meanwhile, the controller module processes these features with the measurement of GNSS locations and angular speed to estimate waypoints that come with latent features. Then, two different agents are used to translate waypoints and latent features into a set of navigational controls to drive the robot. The model is evaluated by predicting driving records and performing automated driving under various conditions in the real environment. Based on the experimental results, DeepIPC achieves the best drivability and multi-task performance even with fewer parameters compared to the other models.

## I. INTRODUCTION

End-to-end learning has become a preferable approach in autonomous driving as manual configuration to integrate task-specific modules is no longer needed. This technique allows the model to share useful features directly from perception parts to controller parts. Besides that, the model can learn and receive extra supervision from a multi-task loss function. All these benefits result in a better model performance even with smaller model size due to its compactness [1][2][3]. To date, there have been a lot of works in the field of end-to-end autonomous driving, whether it is based on simulation [4][5], or offline real world where the model predicts a set of driving records [6][7], or online real world where the model is deployed for automated driving [8][9]. One problem that remains in the online real world autonomous driving is that the model must deal with uncertain conditions including noise and inaccuracy of sensor measurement that affect the model performance [10][11].

To address these issues, several end-to-end models have been proposed with the focus on simulation-to-real adaptation that are incorporating various learning paradigms such as adversarial and reinforcement learning [12][13][14]. Although the models still suffer from performance losses in adapting to uncertain conditions in the real environment, these approaches are said to be promising for future autonomous driving. Different approaches have been proposed

<sup>1</sup>Oskar Natan is with the Department of Computer Science and Engineering, Toyohashi University of Technology, Toyohashi, Aichi 441-8580, Japan, and also with the Department of Computer Science and Electronics, Gadjah Mada University, Yogyakarta 55281, Indonesia. [oskar.natan.ao@tut.jp](mailto:oskar.natan.ao@tut.jp); [oskarnatan@ugm.ac.id](mailto:oskarnatan@ugm.ac.id)

<sup>2</sup>Jun Miura is with the Department of Computer Science and Engineering, Toyohashi University of Technology, Toyohashi, Aichi 441-8580, Japan. [jun.miura@tut.jp](mailto:jun.miura@tut.jp)

with the focus on end-to-end imitation learning where the model is trained to mimic an expert in dealing with uncertainties [15][16][17]. These approaches are preferable as they are easier and can be done with a simple supervised learning.

In this research, we adopt the end-to-end imitation learning approach considering the aforementioned advantages. Moreover, plenty of publicly available datasets [18][19] can be used along with our own dataset to train the model. We design the model based on deep learning architecture that can be forced to learn how to compensate for noisy and inaccurate data. As shown in Fig. 1, the model is equipped with an RGBD camera and other sensors to measure several quantities needed to perceive the environment and drive the robot. This study is a real implementation of our previous work on the simulation-based end-to-end autonomous driving [1]. Therefore, we state the novelty as follows:

- We propose DeepIPC, a deeply integrated perception and control model to drive a mobile robot autonomously in the real environment. The core architecture of DeepIPC is based on our previous work [1]. Then, it is modified to process a wider RGBD input and produce a more maneuverable control with an aim to improve its performance and deal with real implementation issues.
- We compare DeepIPC with other end-to-end models to get a clearer justification. All models are evaluated by performing real automated driving and predicting a set of driving records. Based on the experimental results in two different conditions, DeepIPC achieves the best performance even with fewer parameters.

## II. RELATED WORK

### A. Providing Better Features Through Perception

By completing vision tasks, the perception module can be guided explicitly to provide better features for the controller module as it has the capability of reasoning. Perception can be achieved by performing different kinds of vision tasks such as semantic segmentation, depth estimation, and object detection [20][21]. Specifically, in the field of driving perception, Chiu et. al. [22] proposed a semantic segmentation model that takes a sequence input for a better prediction. Different work is proposed by Rajaram et. al. [23] where a model called RefineNet is used to perform object detection. Besides completing a single vision task, the model can be pushed further to perform multiple vision and control tasks simultaneously to achieve a better understanding and controllability. Recent progress is made by Chitta et. al. [24] where an end-to-end model called AIM-MT (auto-regressive

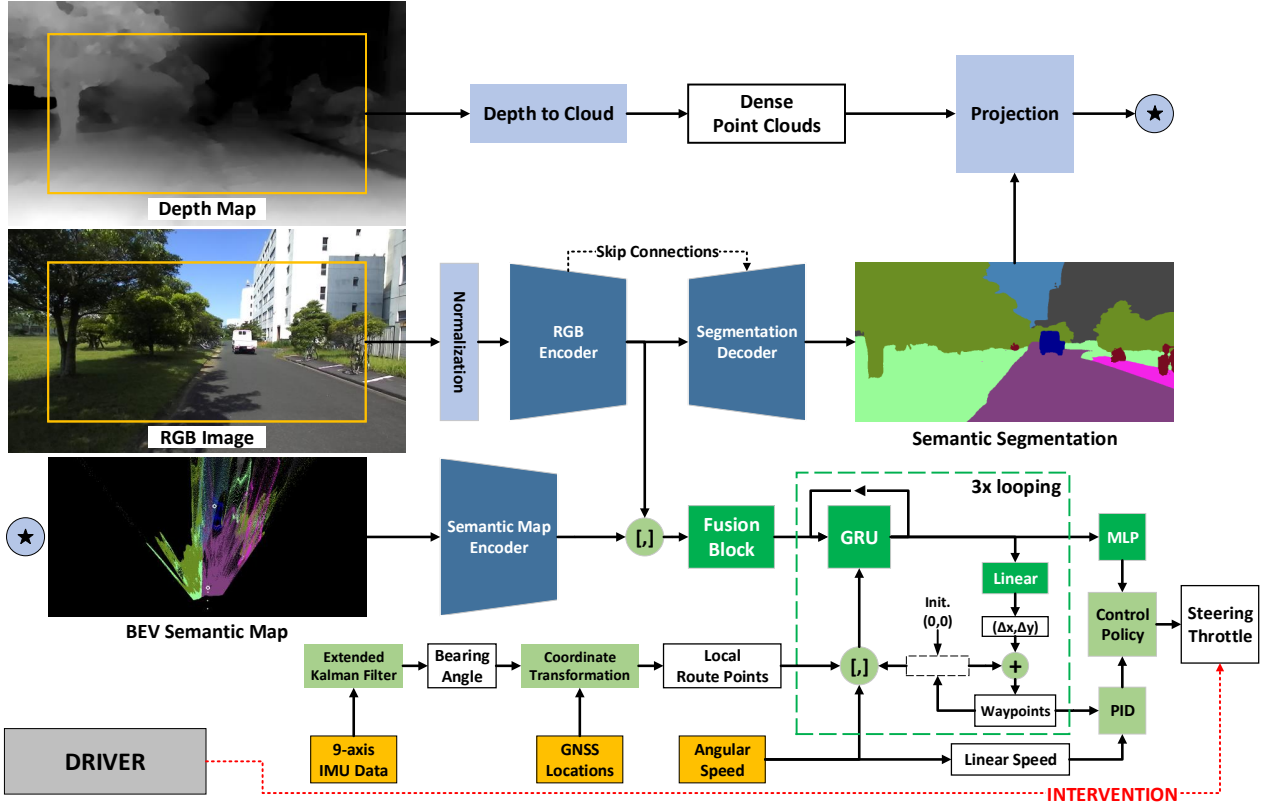


Fig. 1: The architecture of DeepIPC. Blue blocks are considered as part of the perception module, while green blocks are considered as part of the controller module. Light-colored blocks are not trainable, while the darker ones are trainable. In the BEV semantic map, waypoints are denoted with white dots, while route points are denoted with white circles.

image-based model with multi-task supervision) is deployed to perform semantic segmentation and depth estimation while driving a vehicle autonomously.

In this research, we also propose an end-to-end model called DeepIPC that handles perception and control in one forward pass. In contrast to AIM-MT, DeepIPC only uses semantic segmentation as auxiliary supervision since the depth is considered as an input. For comparative study, we use AIM-MT as a representative of the model that uses depth as extra supervision to guide its perception module in providing better features. Thus, the objective is to compare a model with better features against a model with better inputs.

#### B. Fusion-based Model

Processing one kind of data modality is not reliable for autonomous driving as it can be failed under certain conditions. Therefore, more heterogeneous data is needed to cover each other's weaknesses and produce more meaningful information through sensor fusion techniques [25][26]. In the use of RGB image and depth map for autonomous driving, Xiao et. al. [27] demonstrated how these inputs can be fused with different fusion strategies. Another work is proposed by Huang et. al. [28] where RGB image and depth map are fused and extracted from the early perception stage to provide better features for the controller. Besides pixel-to-pixel fusion, the depth map can be used to produce a

BEV semantic map by doing projection with the predicted segmentation map as in our previous work [1]. Thus, the model can perceive from the top view perspective.

Along with AIM-MT, we also use Huang et. al.'s model for comparative study with the objective of comparing the performance of two different sensor fusion strategies. Huang et. al. fuse the information by processing RGB and depth at the early stage to extract a deeper relation on each pixel. Meanwhile, similar to our previous work [1], DeepIPC fuses the information by performing BEV semantic mapping to get the advantage of perceiving from different perspectives.

### III. METHODOLOGY

In this section, we explain the model in detail, especially on how the perception and controller modules work. Then, we describe the dataset used to train, validate, and test the model. Finally, we describe training and evaluation setting including the metrics used to justify the model performance.

#### A. Proposed Model

As mentioned in Section I, the architecture of DeepIPC is based on our previous work [1] that is composed of perception and controller as shown in Fig. 1. The perception phase begins with semantic segmentation on RGB image with a standard encoder-decoder network enhanced with several skip connections [29][30]. The RGB encoder is made

of Efficient Net B3 [31] pre-trained on ImageNet [18], hence a normalization process is necessary. Meanwhile, the decoder is composed of multiple convolution blocks where each block consists of ( $2 \times (3 \times 3)$  convolution + batch normalization + ReLU) + bilinear interpolation and a pointwise  $1 \times 1$  convolution followed with a sigmoid activation. Furthermore, we generate point clouds from the depth map and do projection with the predicted segmentation map to obtain BEV semantic map. Then, the BEV semantic map is encoded by an encoder based on Efficient Net B1 architecture [31] to obtain rich latent features of perception from the BEV perspective.

In the controller module, both RGB and BEV semantic features are processed by a fusion block module which is composed of pointwise ( $1 \times 1$ ) convolution, global average pooling, and linear layer. This module is responsible for learning the relation between features from the front and top view perspectives and resulting in more compact latent features. Then, a gated recurrent unit (GRU) [32] is used to decode the latent features based on the measurement of the left and right wheel's angular speed, predicted waypoints, and two route points that have been transformed into local BEV coordinate. The decoded features are processed further by a linear layer to predict  $\Delta x$  and  $\Delta y$ . Thus, the next waypoint coordinate can be calculated with (1).

$$x_{i+1}, y_{i+1} = (x_i + \Delta x), (y_i + \Delta y) \quad (1)$$

To be noted, the waypoints prediction process is looped over three times as there are three waypoints to be predicted. In the first loop, the waypoint is initialized with the robot position in the local BEV coordinate which is always at (0,0). In the end, the waypoints are translated into a set of navigational controls (steering and throttle) by two PID controllers in which their  $K_p, K_i, K_d$  parameters are tuned empirically. The final features used to predict the last waypoint are also processed by a multi-layer perceptron (MLP) block to estimate the navigational controls directly. The final action that actually drives the robot is made by a control policy that combines both PID and MLP controls as shown in Algorithm 1. We set a confidence threshold of 0.1 as a minimum requirement for an agent to be able to drive the robot. This means that the prediction output on each navigational control must be greater than or equal to 0.1. This mechanism allows an agent to take control completely over the other agent and results in better maneuverability.

### B. Model Modification and Improvement

Different from our previous work [1], the model is modified to improve its performance and deal with real implementation issues. First, as the input to the perception module, we consider a wider ROI of  $H \times W = 512 \times 1024$  at the center of the RGB image and depth map. Then, they are resized to  $H \times W = 256 \times 512$  to reduce the computational load. With a wider input resolution, the model is expected to have a better scene understanding capability. Second, as the input to the controller module, we feed the left and right wheels angular speed instead of the robot's linear speed. This information

---

### Algorithm 1: Control Policy

---

```

 $\Theta = \frac{Wp_1 + Wp_2}{2}; \theta = \tan^{-1} \left( \frac{\Theta[1]}{\Theta[0]} \right)$ 
 $\gamma = 1.75 \times \|Wp_1 - Wp_2\|_F; \nu = \frac{(\omega_l + \omega_r)}{2} \times r$ 
 $\text{PID}_{ST} = \text{PID}^{Lat}(\theta - 90)$ 
 $\text{PID}_{TH} = \text{PID}^{Lon}(\gamma - \nu)$ 
if  $\text{MLP}_{TH} \geq 0.1$  and  $\text{PID}_{TH} \geq 0.1$  then
| if  $|\text{MLP}_{ST}| \geq 0.1$  and  $|\text{PID}_{ST}| < 0.1$  then
| | steering =  $\text{MLP}_{ST}$ 
| else if  $|\text{MLP}_{ST}| < 0.1$  and  $|\text{PID}_{ST}| \geq 0.1$  then
| | steering =  $\text{PID}_{ST}$ 
| else
| | steering =  $\beta_{00}\text{MLP}_{ST} + \beta_{10}\text{PID}_{ST}$ 
| | throttle =  $\beta_{01}\text{MLP}_{TH} + \beta_{11}\text{PID}_{TH}$ 
| else if  $\text{MLP}_{TH} \geq 0.1$  and  $\text{PID}_{TH} < 0.1$  then
| | steering =  $\text{MLP}_{ST}$ ; throttle =  $\text{MLP}_{TH}$ 
| else if  $\text{MLP}_{TH} < 0.1$  and  $\text{PID}_{TH} \geq 0.1$  then
| | steering =  $\text{PID}_{ST}$ ; throttle =  $\text{PID}_{TH}$ 
| else
| | steering = 0; throttle = 0

```

---

$W_{\{1,2\}}$ : first and second waypoints predicted by model  
 $\text{MLP}_{\{ST,TH\}}$ : steering and throttle estimated by MLP agent  
 $\omega_{\{l,r\}}$ : left and right angular speed measured by rotary encoder  
 $r$ : robot's wheel radius, 15 cm  
 $\Theta$ : aim point, a middle point between  $Wp_1$  and  $Wp_2$   
 $\theta$ : heading angle derived from the aim point  $\Theta$   
 $\gamma$ : desired speed,  $1.75 \times$  Frobenius norm of  $Wp_1$  and  $Wp_2$   
 $\nu$ : linear speed, the average of  $\omega_l$  and  $\omega_r$  multiplied by  $r$   
 $\beta \in \{0, \dots, 1\}^{2 \times 2}$  is a set of control weights initialized with:  
 $\beta_{00} = \frac{\alpha_2}{\alpha_2 + \alpha_1}; \beta_{10} = 1 - \beta_{00}$   
 $\beta_{01} = \frac{\alpha_3}{\alpha_3 + \alpha_1}; \beta_{11} = 1 - \beta_{01}$   
where  $\alpha_1, \alpha_2, \alpha_3$  are loss weights computed by MGN algorithm [33] (see Subsection III-D for more details)

---

is expected to be helpful, especially during turning as the angular speed will be different on each wheel. Third, two route points are given instead of one route point which is very risky due to the possibility of mislocation. If the route point is mislocated, the model will fail to predict waypoints and navigational controls correctly. Therefore, giving two route points will make the model have a better intuition in deciding whether the robot should drive straight or turn depending on the location of the route points. Fourth, we also modify the control policy by allowing an agent to take the steering control completely over the other agent. Thus, the robot has better maneuverability during real automated driving.

Unlike the ideal simulation condition, in this research, we equip the model with a GNSS receiver and 9-axis IMU sensor to measure several quantities needed to perform global-to-local coordinate transformation precisely. To get the local BEV coordinate for each route point  $i$ , the relative distance  $\Delta x_i$  and  $\Delta y_i$  between robot location  $Ro$  and route point location  $Rp_i$  must be known. The distance can be estimated from the global longitude-latitude with (2) and (3).

$$\Delta x_i = (Rp_i^{Lat} - Ro^{Lat}) \times \frac{\mathcal{C}_e \times \cos(Ro^{Lat})}{360}, \quad (2)$$

$$\Delta y_i = (Rp_i^{Lon} - Ro^{Lon}) \times \frac{\mathcal{C}_m}{360}, \quad (3)$$



Fig. 2: The experiment area. White circles are an example of a route that consists of start, finish, and route points.

where  $C_e$  and  $C_m$  are earth's equatorial and meridional circumferences which are around 40,075 and 40,008 kilometers, respectively. Then, the exact route point coordinate  $Rp_i^{(x,y)}$  can be obtained by applying a rotation matrix as in (4).

$$\begin{bmatrix} Rp_i^x \\ Rp_i^y \end{bmatrix} = \begin{bmatrix} \cos(\theta_{ro}) & -\sin(\theta_{ro}) \\ \sin(\theta_{ro}) & \cos(\theta_{ro}) \end{bmatrix}^T \begin{bmatrix} \Delta x_i \\ \Delta y_i \end{bmatrix}, \quad (4)$$

where  $\theta_{ro}$  is the robot's absolute orientation to the north pole (bearing angle). We use the Extended Kalman Filter to estimate  $\theta_{ro}$  based on the measurement of 3-axial acceleration, angular speed, and magnetic field retrieved from a 9-axis IMU sensor. Keep in mind that the global-to-local route points transformation may not be so accurate due to the GNSS inaccuracy and noisy IMU measurements. Hence, the model is forced to learn how to compensate for this issue in predicting the waypoints and navigational controls properly.

### C. Dataset

In end-to-end imitation learning, a considerable amount of expert driving records is needed as the dataset for training and validation (train-val) processes [34]. To create the dataset, we drive the robot at a speed of 1.25 m/s in a certain area inside our campus, Toyohashi University of Technology, Japan as shown in Fig. 2 where the left region is used for train-val and the right region is used for test. We consider two experiment conditions which are noon and evening. For each condition, we record the driving data one time for train-val and three times for test. There are 12 routes in the train-val dataset and 6 routes in the test dataset. Each route has a different number of route points since the length is different. The model must follow the route points in driving the robot. The gap between route points is 12 meters and will be changed when the robot is 4 meters close.

The data is recorded at 4 Hz, hence there are four samples retrieved in one second. Each sample consists of an RGB image, depth map, GNSS location, 9-axis IMU measurement, angular speed on the left and the right wheel, and the level of navigational controls (the steering and the throttle). The devices used to retrieve the data are mentioned in Table I, while their placement on the robot can be seen in Fig. 3.

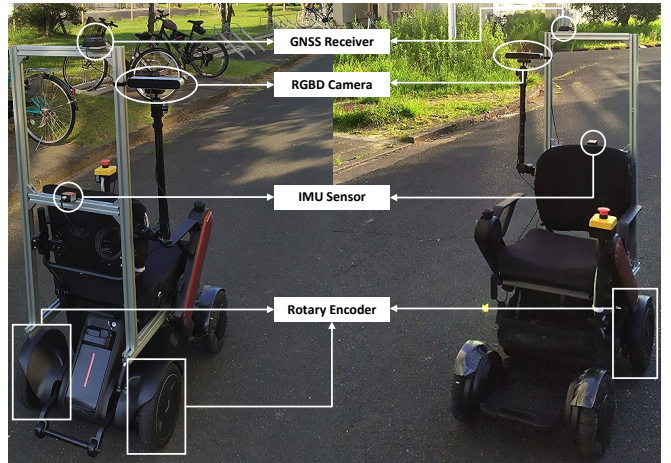


Fig. 3: Sensor placement on the robot. The rotary encoder is mounted inside each rear wheel.

TABLE I: Dataset Information

Conditions	Noon and evening
Total routes	12 (train-val) and 6 (test)
Train frames	4831 (noon), 5320 (evening), 10151 (total)
Val frames	4863 (noon), 4816 (evening), 9679 (total)
Test frames	9510 (noon), 9465 (evening), 18975 (total)
Devices	WHILL model C2 mobile robot Stereolabs Zed 2 RGBD camera U-blox Zed-F9P GNSS receiver Witmotion HWT905 9-axis IMU sensor WHILL's rotary encoder
Object classes	None, road, sidewalk, building, wall, fence, pole, traffic light, traffic sign, vegetation, terrain, sky, person, rider, car, truck, bus, train, motorcycle, bicycle

As mentioned in Subsection III-A, DeepIPC predicts waypoints, navigational controls, and semantic segmentation map. As for waypoints ground truth, we leverage the robot's trajectory where the robot's location in one second, two seconds, and three seconds in the future are considered as the waypoints to be predicted. Meanwhile, navigational controls ground truth can be obtained from the record of steering and throttle levels. To avoid time-consuming manual annotation in producing segmentation ground truth, we use SegFormer [35] trained on Cityscapes dataset [19] to perform segmentation on all RGB images in twenty different classes as mentioned in Table I. SegFormer is chosen as it is considered the current state-of-the-art in the semantic segmentation task.

### D. Training

With multi-task learning strategy, DeepIPC can be supervised by a combination of weighted loss functions as in (5).

$$\mathcal{L}_{MTL} = \alpha_0 \mathcal{L}_{SEG} + \alpha_1 \mathcal{L}_{WP} + \alpha_2 \mathcal{L}_{ST} + \alpha_3 \mathcal{L}_{TH}, \quad (5)$$

TABLE II: Model Specification

Model	Total Parameters ↓	Model Size ↓	Input/Sensor	Output
Huang et. al. [28]	74953258	300.196 MB	RGBD, High-level commands	Segmentation, Steering, Throttle
AIM-MT [24]	27967063	112.078 MB	RGB, GNSS, 9-axis IMU, Rotary encoder	Segmentation, Depth, Waypoints, Steering, Throttle
DeepIPC	20983128	84.972 MB	RGBD, GNSS, 9-axis IMU, Rotary encoder	Segmentation, BEV Semantic, Waypoints, Steering, Throttle

We cannot compute the inference speed fairly due to fluctuating GPU computation, hence we assume that smaller models will infer faster. AIM-MT [24] is implemented based on the codes shared in the author's GitHub repository. Meanwhile, Huang et. al.'s model [28] is implemented independently based on the explanation written in the paper. For a fair comparison, we slightly modify the architecture on both models to process the same information as provided to DeepIPC.

where  $\alpha_{0,1,2,3}$  are loss weights tuned adaptively by an algorithm called modified gradient normalization (MGN) [33] to ensure that all tasks can be learned at the same rate. To learn semantic segmentation, we use a combination of pixel-wise cross entropy and dice loss as in (6).

$$\mathcal{L}_{SEG} = \left( \frac{1}{N} \sum_{i=1}^N y_i \log(\hat{y}_i) + (1 - y_i) \log(1 - \hat{y}_i) \right) + \left( 1 - \frac{2|\hat{y} \cap y|}{|\hat{y}| + |y|} \right), \quad (6)$$

where  $N$  is the total elements at the last layer of the segmentation decoder, while  $y_i$  and  $\hat{y}_i$  are ground truth and prediction of element  $i$ . Then, we use L1 loss to supervise waypoints prediction as in (7).

$$\mathcal{L}_{WP} = \frac{1}{M} \sum_{i=1}^M |\hat{y}_i - y_i|, \quad (7)$$

where  $M$  is equal to 6 as there are three predicted waypoints that have x,y coordinates for each. Similarly, we also use L1 loss to supervise navigational controls prediction as in (8). However, averaging is not needed as there is only one element for each output (steering and throttle).

$$\mathcal{L}_{\{ST, TH\}} = |\hat{y} - y| \quad (8)$$

The model is trained on NVIDIA RTX 3090 GPU with a batch size of 8. We use Adam optimizer [36] with decoupled weight decay of 0.001 [37]. The initial learning rate is set to 0.0001 and divided by 2 if validation  $\mathcal{L}_{MTL}$  is not dropping in 5 epochs in a row. To prevent excessive computation cost, the training is stopped if there is no performance improvement in 30 epochs in a row.

### E. Evaluation and Scoring

As explained in Subsection III-C, the model is evaluated under two different conditions with varying cloud intensity. For each condition, the final score is averaged over three experimental results. We consider two different tests namely offline and online tests. In the offline test, the model is deployed to predict driving records. Then, its performance on each task is calculated by a specific metric function. To evaluate waypoints and navigational controls prediction, we use mean absolute error (MAE) or L1 loss as in (7) and (8). Meanwhile, we compute intersection over union (IoU) as in (9) for evaluating the segmentation performance.

### Algorithm 2: Route points to Commands

---

```

if  $Rp_1^x \leq -4m$  or  $Rp_2^x \leq -8m$  then
| command = turn left
else if  $Rp_1^x \geq 4m$  or  $Rp_2^x \geq 8m$  then
| command = turn right
else
| command = go straight

```

---

$Rp_{\{1,2\}}^x$ : the route point's  $x$  position in local BEV coordinate

$$IoU_{SEG} = \frac{|\hat{y} \cap y|}{|\hat{y} \cup y|} \quad (9)$$

In the online test, the model is deployed to drive a mobile robot by following a set of routes. Unlike in our previous work [1], the robot is prevented from colliding with other objects as it can cause unnecessary damage cost. Therefore, we determine the drivability score by counting the number and time of intervention needed to prevent collisions.

In addition, we conduct a comparative study with some recent models to get a clearer performance justification. We evaluate a model proposed by Huang et. al. [28] that also takes RGB image and depth map but with a different fusion strategy as mentioned in Subsection II-B. However, this model uses high-level commands in selecting a command-specific controller. For a fair comparison, we generate these commands based on the route points using a certain rule as described in Algorithm 2. Then, we also evaluate AIM-MT [24] which only takes RGB as its main input and predicts depth for extra supervision as mentioned in Subsection II-A. By performing more vision tasks, the perception module can be guided explicitly to provide better features for the controller. The model specification details can be seen on Table II. We define the best model by the lowest total metric score (10) that combines semantic segmentation IoU and navigational controls MAE. Depth and waypoints MAE are excluded because not every model has these outputs.

$$TM = (1 - IoU_{SEG}) + MAE_{ST} + MAE_{TH} \quad (10)$$

## IV. RESULT AND DISCUSSION

The offline and online test results can be seen in Table III and Table IV respectively. Meanwhile, several driving records are shown in Fig. 4.

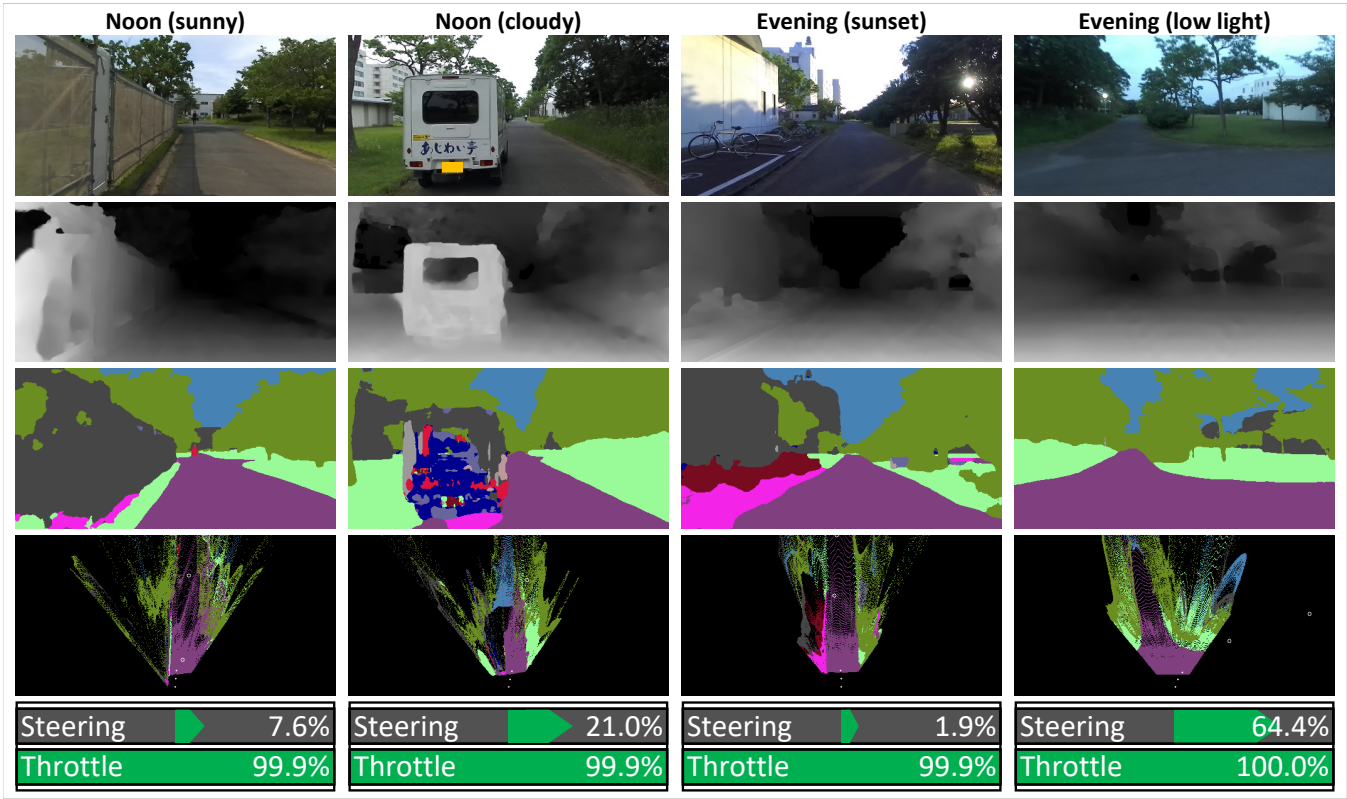


Fig. 4: Driving footage. In the sunny noon, the model makes a small steering adjustment to the right as the robot is too close to the terrain on the left. In the cloudy noon, although the model cannot segment the car properly, it still can avoid collision by going to the right because it knows that the left side is occupied. In the sunset evening, the model makes a small steering adjustment to keep on its lane. In the low light evening, the model makes a right turn following the local position of the first and second route points. See the attached video or <https://youtu.be/h8IMCzJsbi8> for more details.

TABLE III: Multi-task Performance Score

Condition	Model	Total Metric $\downarrow$	$IoU_{SEG} \uparrow$	$MAE_{DE} \downarrow$	$MAE_{WP} \downarrow$	$MAE_{ST} \downarrow$	$MAE_{TH} \downarrow$
Noon	Huang et. al. [28]	$0.4778 \pm 0.0281$	0.8300	-	-	0.2422	0.0484
	AIM-MT [24]	$0.2932 \pm 0.0300$	0.8863	0.0593	0.0983	0.1734	<b>0.0061</b>
	<b>DeepIPC</b>	<b><math>0.2807 \pm 0.0335</math></b>	<b>0.8899</b>	-	<b>0.0683</b>	<b>0.1632</b>	0.0074
Evening	Huang et. al. [28]	$0.4875 \pm 0.0453$	0.7952	-	-	0.2384	0.0443
	AIM-MT [24]	$0.3088 \pm 0.0346$	0.8578	0.0669	0.0931	0.1639	<b>0.0026</b>
	<b>DeepIPC</b>	<b><math>0.3030 \pm 0.0369</math></b>	<b>0.8623</b>	-	<b>0.0645</b>	<b>0.1611</b>	0.0041

The best performance is defined by the lowest total metric score.  $IoU_{SEG}$ : IoU score of semantic segmentation.  $MAE_{DE}$ : mean absolute error of depth estimation. The depth output is normalized from 0.2 to 40 meters to 0 to 1.  $MAE_{WP}$ : mean absolute error of waypoints prediction.  $MAE_{ST}$ : mean absolute error of steering estimation.  $MAE_{TH}$ : mean absolute error of throttle estimation.

#### A. Offline Test

The purpose of the offline test is to evaluate the model’s performance in handling multiple perception and control tasks simultaneously. All models are deployed to make inferences on the test dataset and evaluated with multi-task and task-wise scoring. The test dataset is recorded three times in a completely different area from the train-val dataset. Each record is taken on different days to vary the situation and cloud intensity.

Table III shows that DeepIPC achieves the best performance by having the lowest total metric score in all conditions. However, all models including DeepIPC have performance degradation in the evening. This means that doing inference in the low light condition is harder than in the normal condition. Specifically, in the segmentation task, DeepIPC has a higher IoU than AIM-MT even though it does not perform depth estimation for extra supervision that can enhance the RGB encoder. Thanks to the end-to-end learning

TABLE IV: Drivability Score

Condition	Model	Intervention↓	
		Count	Time (secs)
Noon	Huang et. al. [28]	$1.8889 \pm 0.4157$	$5.6039 \pm 1.7272$
	AIM-MT [24]	$2.2778 \pm 0.3425$	$4.2161 \pm 0.8380$
	<b>DeepIPC</b>	<b><math>1.1111 \pm 0.3928</math></b>	<b><math>2.3092 \pm 0.9841</math></b>
Evening	Huang et. al. [28]	<b><math>1.6111 \pm 0.2079</math></b>	$4.5532 \pm 0.2160$
	AIM-MT [24]	$2.6667 \pm 0.1361$	$4.6736 \pm 0.4293$
	<b>DeepIPC</b>	$1.8889 \pm 0.3928$	<b><math>4.2286 \pm 0.6102</math></b>

The best performance is defined by the lowest intervention count and intervention time.

strategy where the segmentation prediction can be processed further through the encoding and decoding process of the BEV semantic map. Therefore, the segmentation decoder receives a more useful gradient signal to tune the network weights properly. Meanwhile, Huang et. al.'s model has the worst segmentation performance that is caused by conflicting features as its perception module fuses RGB image and depth map from the early perception stage.

In the waypoints prediction task, DeepIPC has a lower MAE compared to AIM-MT. Thanks to the BEV semantic features, DeepIPC has a better capability in perceiving free and occupied areas from the top view perspective. Thus, it can easily estimate the waypoints which are also laid in BEV space. Keep in mind that although AIM-MT predicts four waypoints and DeepIPC only predicts three waypoints, it is still considered a fair comparison because the MAE formula averages the error across all predicted waypoints. The reason the AIM-MT predicts four waypoints is to let its controller module have more learning experiences in estimating the waypoints correctly. However, DeepIPC still performs better as its controller module gets boosted by BEV semantic features and fed with angular speed measurement that enhances its intuition. This result is in line with the result in our previous work [1] where the model that perceives in BEV perspective (by using depth projection or LiDAR) is better at estimating the waypoints than the model that perceives in front view perspective only.

In the navigational controls estimation task, DeepIPC also has the best performance in line with the waypoints prediction result. The MLP agent can leverage useful features encoded from both RGB and BEV semantic map. Therefore, the MLP agent can perform as good as the PID agent in estimating steering and throttle. With two different agents considering various aspects of driving, more appropriate action can be decided. Compared to AIM-MT, DeepIPC is better at estimating the steering but worse at estimating the throttle. Yet, it can be said that DeepIPC is better than AIM-MT considering that better steering control is more important than better throttle control in low-speed driving. Meanwhile, Huang et. al.'s model is far behind the others in estimating navigational controls. The model has a action-specific controller for each command ("go straight", "turn left", "turn right") that fails to adapt on diverse situations.

### B. Online Test

The purpose of the online test is to evaluate the model's drivability in driving a mobile robot in the real environment. The model must be able to drive the robot safely by following a set of routes while avoiding obstacles (e.g., a vehicle stopped on the left side of the road). The experiment is conducted three times in noon and evening conditions. Each experiment is conducted on different days, hence the robot can experience various situations. The performance is evaluated based on the average intervention count and intervention time. Concisely, the less the driver does intervention means the better the driving performance. For a fair comparison, the experiments for all models are monitored by the same driver. Thus, each intervention is based on the same perspective of the degree of danger in preventing the collision.

Table IV shows that DeepIPC achieves the best drivability at noon where it has the lowest intervention count and intervention time. Meanwhile, DeepIPC is comparable to Huang et. al.'s model in the evening where it achieves the lowest intervention time but higher intervention count. Keep in mind that a model with a lower intervention count can have a longer intervention time. For example, a model that fails to make a turn and going to collide with terrain or sidewalk is need more correction time than a model that makes a small deviation on a straight path. Hence, it depends on the degree of danger in which the collision is going to happen. Based on the intervention time per intervention count, it is obvious that Huang et. al.'s model needs more correction time for each intervention. This means that it has the highest danger level. Meanwhile, DeepIPC and AIM-MT only need less intervention time in low-degree dangerous situations.

In a comparison between drivability at noon and evening, DeepIPC and AIM-MT get their performance degraded in the evening as they only process RGB image at the early perception stage. On the contrary, Huang et. al.'s model achieves a better performance meaning that the early fusion strategy is useful for driving in the low light condition.

## V. CONCLUSIONS

We present DeepIPC, a deeply integrated perception and control model for driving a mobile robot in the real environment. The model is evaluated by predicting a set of driving records (offline test) and performing automated driving (online test). Furthermore, a comparative study with some recent models is conducted to justify its performance.

Based on the experimental results, we disclosed several findings as follows. First, BEV semantic features can improve the model performance in predicting waypoints and navigational controls. With a better perception, the model can leverage useful information which results in better drivability. Second, driving in the low light condition is harder than in the normal condition, especially for DeepIPC and AIM-MT which only rely on RGB image at the early perception stage. Meanwhile, Huang et. al.'s model can tackle this issue as it fuses RGB and depth features earlier. Lastly, considering its performance on both tests and the number of parameters used in its architecture, DeepIPC can be said as the best model.

As for future works, the perception module can be enhanced with a DVS camera and/or LiDAR to handle poor illumination conditions such as nighttime. Then, conducting an evaluation on adversarial situations (e.g., avoiding collision with pedestrians that cross the street suddenly) is suitable for testing the drivability further.

## REFERENCES

- [1] O. Natan and J. Miura, "End-to-end autonomous driving with semantic depth cloud mapping and multi-agent," *IEEE Trans. Intell. Vehicles*, 2022. [Online]. Available: <https://doi.org/10.1109/TIV.2022.3185303>
- [2] A. Tampuu, T. Matiscen, M. Semikin, D. Fishman, and N. Muhammad, "A survey of end-to-end driving: Architectures and training methods," *IEEE Trans. Neural Networks and Learning Syst.*, vol. 33, no. 4, pp. 1364–1384, Apr. 2022.
- [3] L. Le Mero, D. Yi, M. Dianati, and A. Mouzakitis, "A survey on imitation learning techniques for end-to-end autonomous vehicles," *IEEE Trans. Intell. Transp. Syst.*, 2022. [Online]. Available: <https://doi.org/10.1109/TITS.2022.3144867>
- [4] D. Wang, C. Devin, Q.-Z. Cai, F. Yu, and T. Darrell, "Deep object-centric policies for autonomous driving," in *Proc. IEEE Inter. Conf. Robot. and Autom. (ICRA)*, Montreal, Canada, May 2019, pp. 8853–8859.
- [5] K. Ishihara, A. Kanervisto, J. Miura, and V. Hautamaki, "Multi-task learning with attention for end-to-end autonomous driving," in *Proc. IEEE/CVF Conf. Comput. Vision and Pattern Recog. Workshops (CVPRW)*, Nashville, USA, June 2021, pp. 2896–2905.
- [6] Y. Xu, X. Yang, L. Gong, H.-C. Lin, T.-Y. Wu, Y. Li, and N. Vasconcelos, "Explainable object-induced action decision for autonomous vehicles," in *Proc. IEEE/CVF Conf. Comput. Vision and Pattern Recog. (CVPR)*, Seattle, USA, June 2020, pp. 9520–9529.
- [7] T. Wu, A. Luo, R. Huang, H. Cheng, and Y. Zhao, "End-to-end driving model for steering control of autonomous vehicles with future spatiotemporal features," in *Proc. IEEE/RSJ Inter. Conf. Intell. Robots and Syst. (IROS)*, Macau, China, Nov. 2019, pp. 950–955.
- [8] D. Omeiza, H. Web, M. Jiroka, and L. Kunze, "Towards accountability: Providing intelligible explanations in autonomous driving," in *Proc. IEEE Intell. Vehicles Symp. (IV)*, Nagoya, Japan, July 2021, pp. 231–237.
- [9] C. Guo, K. Kidono, R. Terashima, and Y. Kojima, "Humanlike behavior generation in urban environment based on learning-based potentials with a low-cost lane graph," *IEEE Trans. Intell. Vehicles*, vol. 3, no. 1, pp. 46–60, Mar. 2018.
- [10] D. Feng, C. Haase-Schütz, L. Rosenbaum, H. Hertlein, C. Gläser, F. Timm, W. Wiesbeck, and K. Dietmayer, "Deep multi-modal object detection and semantic segmentation for autonomous driving: Datasets, methods, and challenges," *IEEE Trans. Intell. Transp. Syst.*, vol. 22, no. 3, pp. 1341–1360, Mar. 2021.
- [11] V. S. Medeiros, E. Jelavic, M. Bjelonic, R. Siegwart, M. A. Meggiolaro, and M. Hutter, "Trajectory optimization for wheeled-legged quadrupedal robots driving in challenging terrain," *IEEE Robot. and Autom. Lett.*, vol. 5, no. 3, pp. 4172–4179, July 2020.
- [12] W. Yuan, M. Yang, C. Wang, and B. Wang, "VRDriving: A virtual-to-real autonomous driving framework based on adversarial learning," *IEEE Trans. Cognitive and Developmental Syst.*, vol. 13, no. 4, pp. 912–921, Dec. 2021.
- [13] P. Almási, R. Moni, and B. Gyires-Tóth, "Robust reinforcement learning-based autonomous driving agent for simulation and real world," in *Proc. Inter. Joint Conf. Neural Networks (IJCNN)*, Glasgow, UK, July 2020, pp. 1–8.
- [14] A. Amini, I. Gilitschenski, J. Phillips, J. Moseyko, R. Banerjee, S. Karaman, and D. Rus, "Learning robust control policies for end-to-end autonomous driving from data-driven simulation," *IEEE Robot. and Autom. Lett.*, vol. 5, no. 2, pp. 1143–1150, Apr. 2020.
- [15] Y. Cui, D. Isele, S. Niekum, and K. Fujimura, "Uncertainty-aware data aggregation for deep imitation learning," in *Proc. IEEE Inter. Conf. Robot. and Autom. (ICRA)*, Montreal, Canada, May 2019, pp. 761–767.
- [16] J. Zhou, R. Wang, X. Liu, Y. Jiang, S. Jiang, J. Tao, J. Miao, and S. Song, "Exploring imitation learning for autonomous driving with feedback synthesizer and differentiable rasterization," in *Proc. IEEE/RSJ Inter. Conf. Intell. Robots and Syst. (IROS)*, Prague, Czech Republic, Sept. 2021, pp. 1450–1457.
- [17] J. Hawke, R. Shen, C. Gurau, S. Sharma, D. Reda, N. Nikolov, P. Mazur, S. Micklithwaite, N. Griffiths, A. Shah, and A. Kndall, "Urban driving with conditional imitation learning," in *Proc. IEEE Inter. Conf. Robot. and Autom. (ICRA)*, Paris, France, Aug. 2020, pp. 251–257.
- [18] J. Deng, W. Dong, R. Socher, L.-J. Li, K. Li, and L. Fei-Fei, "ImageNet: A large-scale hierarchical image database," in *Proc. IEEE/CVF Conf. Comput. Vision and Pattern Recog. (CVPR)*, Miami, USA, June 2009, pp. 248–255.
- [19] M. Cordts, M. Omran, S. Ramos, T. Rehfeld, M. Enzweiler, R. Benenson, U. Franke, S. Roth, and B. Schiele, "The cityscapes dataset for semantic urban scene understanding," in *Proc. IEEE/CVF Conference on Comput. Vision and Pattern Recog. (CVPR)*, Las Vegas, USA, June 2016, pp. 3213–3223.
- [20] B. Ranft and C. Stiller, "The role of machine vision for intelligent vehicles," *IEEE Trans. Intell. Vehicles*, vol. 1, no. 1, pp. 8–19, Mar. 2016.
- [21] E. Alberti, A. Tavera, C. Masone, and B. Caputo, "IDDA: A large-scale multi-domain dataset for autonomous driving," *IEEE Robot. and Autom. Lett.*, vol. 5, no. 4, pp. 5526–5533, Oct. 2020.
- [22] H.-k. Chiu, E. Adeli, and J. C. Niebles, "Segmenting the future," *IEEE Robot. and Autom. Lett.*, vol. 5, no. 3, pp. 4202–4209, July 2020.
- [23] R. N. Rajaram, E. Ohn-Bar, and M. M. Trivedi, "RefineNet: Refining object detectors for autonomous driving," *IEEE Trans. Intell. Vehicles*, vol. 1, no. 4, pp. 358–368, Dec. 2016.
- [24] K. Chitta, A. Prakash, and A. Geiger, "NEAT: Neural attention fields for end-to-end autonomous driving," in *Proc. IEEE/CVF Inter. Conf. Comput. Vision (ICCV)*, Montreal, Canada, Oct. 2021, pp. 15773–15783.
- [25] S. Fang and A. Choromanska, "Multi-modal experts network for autonomous driving," in *Proc. IEEE Inter. Conf. Robot. and Autom. (ICRA)*, Paris, France, Aug. 2020, pp. 6439–6445.
- [26] N. Patel, A. Choromanska, P. Krishnamurthy, and F. Khorrami, "Sensor modality fusion with cnns for ugv autonomous driving in indoor environments," in *Proc. IEEE/RSJ Inter. Conf. Intell. Robots and Syst. (IROS)*, Vancouver, Canada, Sept. 2017, pp. 1531–1536.
- [27] Y. Xiao, F. Codevilla, A. Gurram, O. Urfalioglu, and A. M. López, "Multimodal end-to-end autonomous driving," *IEEE Trans. Intell. Transp. Syst.*, vol. 23, no. 1, pp. 537–547, Jan. 2022.
- [28] Z. Huang, C. Lv, Y. Xing, and J. Wu, "Multi-modal sensor fusion-based deep neural network for end-to-end autonomous driving with scene understanding," *IEEE Sensors J.*, vol. 21, no. 10, pp. 11781–11790, May 2021.
- [29] O. Natan, D. U. K. Putri, and A. Dharmawan, "Deep learning-based weld spot segmentation using modified UNet with various convolutional blocks," *ICIC Express Lett. Part B: Applications*, vol. 12, no. 12, pp. 1169–1176, Dec. 2021.
- [30] O. Natan and J. Miura, "Semantic segmentation and depth estimation with RGB and DVS sensor fusion for multi-view driving perception," in *Proc. Asian Conf. Pattern Recog. (ACPR)*, Jeju Island, South Korea, Nov. 2021, pp. 352–365.
- [31] M. Tan and Q. Le, "EfficientNet: Rethinking model scaling for convolutional neural networks," in *Proc. Inter. Conf. Machine Learning (ICML)*, Long Beach, USA, June 2019, pp. 6105–6114.
- [32] K. Cho, B. van Merriënboer, D. Bahdanau, and Y. Bengio, "On the properties of neural machine translation: Encoder-decoder approaches," in *Proc. Workshop Syntax, Semantics and Structure in Statistical Translation (SSST)*, Doha, Qatar, Oct. 2014, pp. 103–111.
- [33] O. Natan and J. Miura, "Towards compact autonomous driving perception with balanced learning and multi-sensor fusion," *IEEE Trans. Intell. Transp. Syst.*, 2022. [Online]. Available: <https://doi.org/10.1109/TITS.2022.3149370>
- [34] A. O. Ly and M. Akhlaoufi, "Learning to drive by imitation: An overview of deep behavior cloning methods," *IEEE Trans. Intell. Vehicles*, vol. 6, no. 2, pp. 195–209, June 2021.
- [35] E. Xie, W. Wang, Z. Yu, A. Anandkumar, J. M. Alvarez, and P. Luo, "SegFormer: Simple and efficient design for semantic segmentation with transformers," in *Proc. Inter. Conf. Neural Information Processing Syst. (NIPS)*, Online, Dec. 2021, pp. 1–18.
- [36] D. P. Kingma and J. Ba, "Adam: A method for stochastic optimization," in *Proc. Inter. Conf. Learning Representations (ICLR)*, San Diego, USA, May 2015, pp. 1–15.
- [37] I. Loshchilov and F. Hutter, "Decoupled weight decay regularization," in *Proc. Inter. Conf. Learning Representations (ICLR)*, New Orleans, USA, May 2019, pp. 1–10.